

Tunable Noise Cross-Correlations in a Double Quantum Dot

D. T. McClure, L. DiCarlo, Y. Zhang, H.-A. Engel and C. M. Marcus
Department of Physics, Harvard University, Cambridge, Massachusetts 02138, USA

M. P. Hanson and A. C. Gossard
Department of Materials, University of California, Santa Barbara, California, 93106, USA
 (Dated: April 18, 2018)

We report measurements of the cross-correlation between current noise fluctuations in two capacitively coupled quantum dots in the Coulomb blockade regime. The sign of the cross-spectral density is found to be tunable by gate voltage and source-drain bias. Good agreement is found with a model of sequential tunneling through the dots in the presence of inter-dot capacitive coupling.

Current noise cross-correlation in mesoscopic electronics is of broad interest because it is sensitive to quantum indistinguishability and interactions [1, 2, 3, 4, 5]. In the absence of interactions, Pauli exclusion makes the cross-correlation between any two outgoing currents negative, regardless of device geometry, temperature, and bias voltage [6]. Experiments to date, notably the electronic versions of the Hanbury Brown-Twiss experiment [7, 8, 9], have shown good agreement with this theoretical prediction.

However, the negative sign of the cross-correlation rests on a number of assumptions: a low-impedance external circuit, low measurement frequency, and vanishing interactions. Recent work [10, 11, 12, 13, 14] explores the possibility of controlling the sign of cross-correlations by relaxing one or more of these conditions. For example, if the first assumption is relaxed, sign reversal can result from strong inelastic scattering, as theoretically predicted [10] and experimentally demonstrated [13] using a voltage probe. Furthermore, sign reversal can also occur in hybrid superconductor-normal systems when non-local Andreev reflection dominates over normal scattering, as was shown theoretically in Refs. [15, 16, 17].

In this Letter, we report gate-controlled sign reversal of noise cross-correlation due to strong Coulomb interaction in a capacitively coupled double quantum dot. Previously, super-Poissonian current noise was observed in mesoscopic tunnel junctions [18] and silicon MOSFETs at low transmission [19] and attributed to Coulomb interaction between localized states mediating transport. In contrast to devices with uncontrolled localized states, the present structure allows full control of Coulomb-induced correlation via the electrostatic gates that define the two dots. A model of sequential tunneling through a single level within each dot that includes capacitive coupling yields good agreement with the experimental results. This study provides an intuitive picture of how Coulomb interaction influences noise cross-correlation, taking advantage of a well-controlled device geometry.

The four-terminal double-dot device is defined by top gates on the surface of a GaAs/Al_{0.3}Ga_{0.7}As heterostructure grown by molecular beam epitaxy [see micrograph

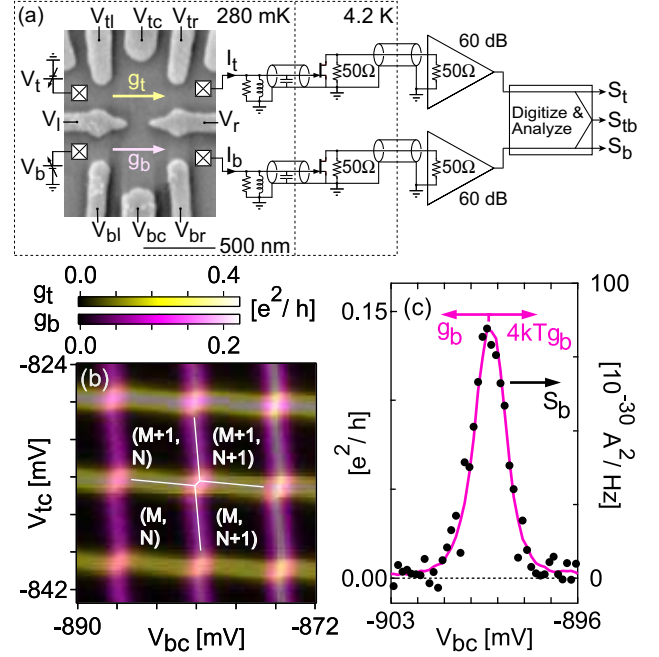


FIG. 1: (a) Scanning electron micrograph of the double-dot device, and equivalent circuit at 2 MHz of the noise detection system measuring the power spectral densities and cross spectral density of fluctuations in currents I_t and I_b . (b) Differential conductances g_t (yellow) and g_b (magenta) as a function of V_{tc} and V_{bc} over a few Coulomb blockade peaks in each dot, at $V_t = V_b = 0$. Black regions correspond to well-defined charge states in the double-dot system. Superimposed white lines indicate the honeycomb structure resulting from the finite inter-dot capacitive coupling. (c) Zero-bias (thermal) noise S_b (black dots, right axis), conductance g_b (magenta curve, left axis), and calculated $4k_B T_e g_b$ (magenta curve, right axis) as a function of gate voltage V_{bc} .

in Fig. 1(a)]. The two-dimensional electron gas 100 nm below the surface has a density of $2 \times 10^{11} \text{ cm}^{-2}$ and mobility $2 \times 10^5 \text{ cm}^2/\text{Vs}$. Throughout this experiment, gate voltages $V_l = V_r = -1420 \text{ mV}$ fully deplete the central point contact such that the dots are coupled only capacitively, not via tunneling. Gate voltages V_{tl} (V_{bl}) and V_{tr} (V_{br}) control the tunnel barrier between the top (bottom) dot and its left and right leads. Plunger gate voltage V_{tc} (V_{bc}) controls the electron number M (N) in

the top (bottom) dot; for this experiment $M \sim N \sim 100$. The lithographic area of each dot is $0.15 \mu\text{m}^2$. We estimate a mean level spacing of each dot $\Delta_{t(b)} \approx 70 \mu\text{eV}$, assuming $\sim 100 \text{ nm}$ of lateral depletion around the gates.

Measurements are carried out in a ^3He cryostat equipped with a two-channel noise measurement system [20], shown schematically in Fig. 1(a). A voltage bias V_t (V_b) is applied to the left lead of the top (bottom) dot, with right leads held at ground. Separate resistor-inductor-capacitor resonators ($R = 5 \text{ k}\Omega$, $L = 66 \mu\text{H}$, $C = 96 \text{ pF}$) convert fluctuations in currents I_t and I_b through the top and bottom dots around 2 MHz into voltage fluctuations on gates of high electron mobility transistors (HEMTs) at 4.2 K , which in turn convert these into current fluctuations in two 50Ω coaxial lines extending to room temperature, where further amplification is performed. These signals are then simultaneously digitized at 10 MHz , their fast Fourier transforms calculated, and the current noise power spectral densities S_t , S_b and cross-spectral density S_{tb} extracted. The overall gain of each amplification channel and the base electron temperature $T_e = 280 \text{ mK}$ are calibrated *in situ* using Johnson-noise thermometry at base temperature and 1.6 K with the device configured as two point contacts [20]. Differential conductance g_t (g_b) through the top (bottom) dot is measured using standard lock-in technique with an applied excitation of 25 (30) μV_{rms} at 677 (1000) Hz . Ohmic contact resistances of roughly a few $\text{k}\Omega$, much smaller than the dot resistances, are not subtracted.

Superposed top and bottom dot conductances g_t and g_b as a function of plunger voltages V_{tc} and V_{bc} form the characteristic double-dot honeycomb pattern [21, 22], with dark regions corresponding to well-defined electron number in each dot, denoted (M, N) (first index for top dot), as shown in Fig. 1(b). Horizontal (vertical) features in g_t (g_b) are Coulomb blockade (CB) conductance peaks [23], across which M (N) increases by one as V_{tc} (V_{bc}) is raised. The distance between triple points, i.e., the length of the short edge of the hexagon, provides a measure of the mutual charging energy U due to inter-dot capacitive coupling. By comparing this distance to the CB peak spacing, and using the single-dot charging energy $E_C = 600 \mu\text{eV}$ extracted from finite bias CB diamonds (not shown), we estimate $U \approx 60 \mu\text{eV}$ [22]. We refer to the midpoint of the short edge of the hexagon, midway between triple points, as the “honeycomb vertex.” Current noise S_b and conductance g_b , measured simultaneously around zero-bias, over a CB peak in the bottom dot (with the top dot in a CB valley) are shown in Fig. 1(c). Good agreement between the measured S_b and the Johnson-Nyquist thermal noise value $4k_B T_e g_b$ is observed.

Turning now to finite-bias noise measurements, Fig. 2(a) shows the measured noise cross-correlation S_{tb} as a function of plunger gate voltages V_{tc} and V_{bc} in

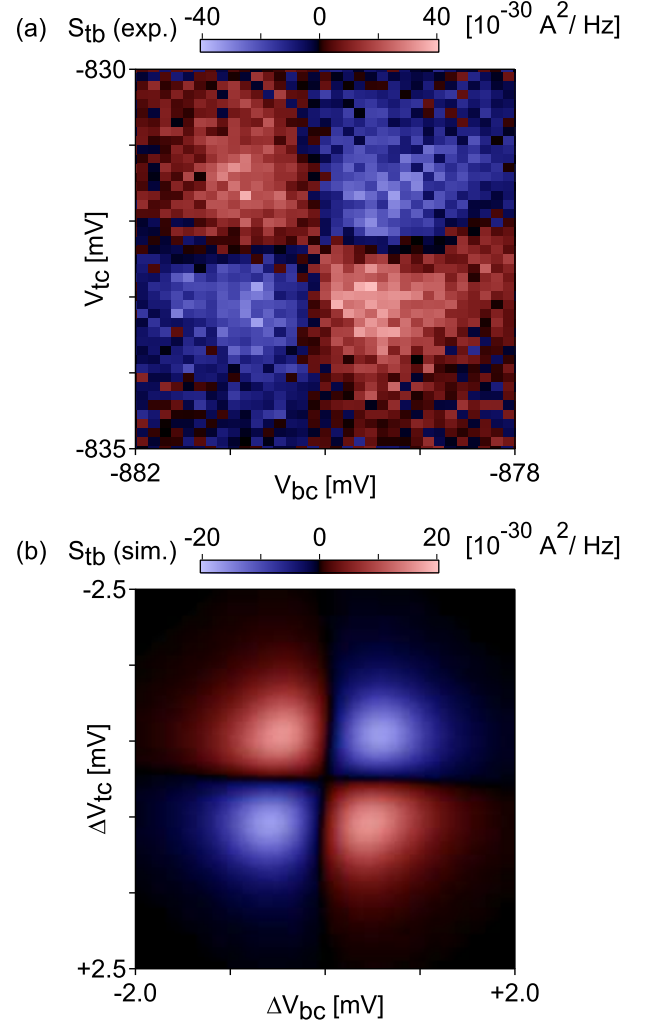


FIG. 2: Measured (a) and simulated (b) cross-spectral density S_{tb} near a honeycomb vertex, with applied bias $V_t = V_b = -100 \mu\text{V}$ ($e|V_{t(b)}| \approx 4k_B T_e \approx E_C/6$). Blue regions (lower-left and upper-right) indicate negative cross-correlation, while red regions indicate positive cross-correlation.

the vicinity of a honeycomb vertex, with voltage bias of $-100 \mu\text{V}$ applied to both dots. The plot reveals a characteristic quadrupole pattern of noise cross-correlation centered on the honeycomb vertex, comprising both negative and positive cross-correlation regions. The symmetry of this pattern is found to depend rather sensitively on balancing each dot’s left and right tunnel barriers.

To better understand this experimental result, we model the system as single-level dots capacitively coupled by a mutual charging energy U , each with weak tunneling to the leads. The energy required to add electron $M + 1$ to the top dot depends on the two plunger gate voltages as well as the electron number $n \in \{N, N + 1\}$ on the bottom dot: $E_t = \alpha_t V_{tc} + \beta_t V_{bc} + U \cdot n + \text{const.}$, where lever arms α_t and β_t are obtained from the honeycomb diagram in Fig. 1(b) [21] and the measured E_C .

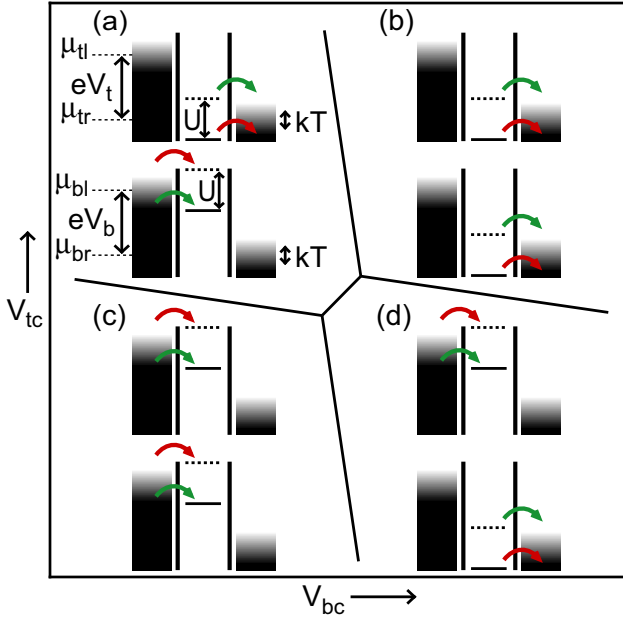


FIG. 3: Energy level diagrams in the vicinity of a honeycomb vertex, with biases $V_{t(b)} = -100 \mu\text{V}$. (The various energies are shown roughly to scale.) The solid horizontal line in the top (bottom) dot represents the energy $E_{t(b)}$ required to add electron $M+1$ ($N+1$) when the bottom (top) dot has N (M) electrons. The dashed horizontal line, higher than the solid line by U , represents $E_{t(b)}$ when the bottom (top) dot has $N+1$ ($M+1$) electrons. In each dot, the rate of either tunneling-in from the left or tunneling-out to the right is significantly affected by this difference in the energy level, taking on either a slow value (red arrow) or a fast value (green arrow) depending on the electron number in the other dot. In (a) and (d), where the occurrence of each U -sensitive process enhances the rate of the other, we find positive cross-correlation. In (b) and (c), where the occurrence of each U -sensitive process suppresses the rate of the other, we find negative cross-correlation.

The energy E_b to add electron $N+1$ to the bottom dot is given by an analogous formula. Occupation probabilities for charge states (M, N) , $(M+1, N)$, $(M, N+1)$, and $(M+1, N+1)$ are given by the diagonal elements of the density matrix, $\rho = (\rho_{00}, \rho_{10}, \rho_{01}, \rho_{11})^T$. The time evolution of ρ is given by a master equation $d\rho/dt = \mathcal{M}\rho$, where

$$\mathcal{M} = \begin{pmatrix} -W_{00}^{\text{out}} & W_{00 \leftarrow 10} & W_{00 \leftarrow 01} & 0 \\ W_{10 \leftarrow 00} & -W_{10}^{\text{out}} & 0 & W_{01 \leftarrow 11} \\ W_{01 \leftarrow 00} & 0 & -W_{01}^{\text{out}} & W_{10 \leftarrow 11} \\ 0 & W_{11 \leftarrow 10} & W_{11 \leftarrow 01} & -W_{11}^{\text{out}} \end{pmatrix}. \quad (1)$$

Each diagonal element of \mathcal{M} gives the total loss rate for the corresponding state, with $W_{\alpha}^{\text{out}} = \sum_{\beta} W_{\beta \leftarrow \alpha}$. Off-diagonal terms give the total rate for transitions between two states. For example, $W_{10 \leftarrow 00} = W_{10 \leftarrow 00}^l + W_{10 \leftarrow 00}^r$ is the total tunneling rate into $(M+1, N)$ from (M, N) , containing tunneling contributions from the top-left and top-right leads.

Rates for tunneling-in and tunneling-out between a dot and either of its leads $i \in \{tl, tr, bl, br\}$ depend on both the transparency Γ^i of the tunnel barrier to lead i and the

Fermi function $f_i(\epsilon) = [1 + \exp\{(\epsilon - \mu_i)/k_B T_e\}]^{-1}$ evaluated at the value at $\epsilon = E_{t(b)}$, where μ_i is the chemical potential in lead i . For example, the rates for tunneling into and out of the top dot from/to the left lead are given by $W_{10 \leftarrow 00}^l = \Gamma^{lt} f_{lt}(E_t)$ and $W_{00 \leftarrow 10}^l = \Gamma^{lt} [1 - f_{lt}(E_t)]$, respectively. As E_t is lowered across μ_{lt} , $W_{10 \leftarrow 00}^l$ increases from 0 to Γ^{lt} over a range of a few $k_B T_e$, while $W_{00 \leftarrow 10}^l$ does the opposite.

We obtain the steady-state value of ρ , denoted $\bar{\rho}$, by solving $d\bar{\rho}/dt = \mathcal{M}\bar{\rho} = 0$. Using techniques described in detail in Refs. [24, 25, 26], we define current matrices J^{tr} and J^{br} for the top-right and bottom-right leads and apply them to $\bar{\rho}$ to calculate the average currents $\langle I_{t(b)} \rangle$ and the correlator $\langle I_t(\tau) I_b(0) \rangle$ [27]. The cross-spectral density in the low-frequency limit is then given by

$$S_{tb} = 2 \int_{-\infty}^{\infty} [\langle I_t(\tau) I_b(0) \rangle - \langle I_t \rangle \langle I_b \rangle] d\tau. \quad (2)$$

Simulation results for noise cross-correlation S_{tb} as a function of plunger gate voltages are shown in Fig. 2(b), with all parameters of the model extracted from experiment: $U = 60 \mu\text{eV}$, $T_e = 280 \text{ mK}$, $\Gamma^{tl} = \Gamma^{tr} = 1.5 \times 10^{10} \text{ s}^{-1}$, and $\Gamma^{bl} = \Gamma^{br} = 7.2 \times 10^9 \text{ s}^{-1}$. The Γ^i were estimated from the zero-bias conductance peak height using Eq. 6.3 from Ref. [28] and assuming symmetric left and right barriers. The simulation shows the characteristic quadrupole pattern of positive and negative cross-correlation observed experimentally. We note that the model underestimates S_{tb} by roughly a factor of two. This may be due to transport through processes not accounted for in the model. Elastic cotunneling may be present since the Γ^i are comparable to $k_B T_e / \hbar$. Furthermore, since the voltage-bias energy $|eV_{t(b)}|$ is greater than the level spacing $\Delta_{t(b)}$, transport may occur via multiple levels [29, 30] and via inelastic cotunneling [31, 32].

Some intuition for how Coulomb interactions affect noise cross-correlation in this device geometry can be gained from simple considerations of energy level positions in the space of plunger gate voltages, illustrated in Fig. 3. With both dots positioned near Coulomb blockade peaks, the fluctuations by one in the electron number of each dot, caused by the sequential tunneling of electrons through that dot, cause the energy level of the other dot to fluctuate between two values separated by U . These fluctuations can raise and lower the level across the chemical potential in one of the dot's leads, strongly affecting either the tunnel-in rate (from the left, for the case illustrated in Fig. 3) or the tunnel-out rate (to the right) of that dot. Specifically, the rate of the “ U -sensitive” process in each dot fluctuates between a slow value (red arrow), suppressed significantly from Γ^i , and a fast value (green arrow), close to Γ^i . Since the Γ^i for the left and right barriers of each dot are roughly equal, the U -sensitive process becomes the rate-limiting process for transport through the dot when its rate is suppressed.

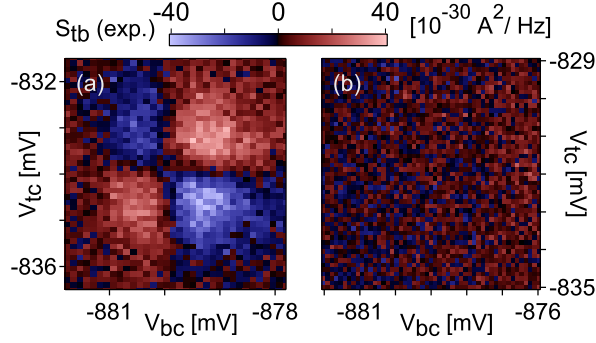


FIG. 4: (a) Measured S_{tb} near a honeycomb vertex, with opposite biases $V_t = -V_b = -100 \mu\text{V}$. Note that the pattern is reversed from Fig. 2(a): negative cross-correlation (blue) is now found in the upper-left and lower-right regions, while positive cross-correlation (red) is now found in the lower-left and upper-right. (b) Measured S_{tb} near a honeycomb vertex, with $V_t = V_b = 0$. Cross-correlation of noise vanishes at zero bias, though the noise in each dot is finite.

The U -sensitive processes correlate transport through the two dots. In region (b) of Fig. 3, for instance, where S_{tb} is negative, the U -sensitive process in each dot is tunneling-out. Here, as well as in (c), where the U -sensitive process in each dot is tunneling-in, the two U -sensitive processes compete: the occurrence of one suppresses the rate of the other, leading to negative S_{tb} . Conversely, in region (a) [(d)], where S_{tb} is positive, the U -sensitive process in the top [bottom] dot is tunneling-out, and in the bottom [top] dot it is tunneling-in. Here, the U -sensitive processes cooperate: the occurrence of one lifts the suppression of the other, leading to positive S_{tb} .

The arguments above also apply when one or both biases are reversed. When both are reversed, we find both experimentally and in the model that the same cross-correlation pattern as in Fig. 2 appears (not shown). When only one of the biases is reversed, we find both experimentally [as shown in Fig. 4(a)] and in the model that the pattern reverses sign. In the absence of any bias, cross-correlation vanishes both experimentally [as shown in Fig. 4(b)] and in the model, despite the fact that noise in the individual dots remains finite (as seen in Fig. 1(c)).

In conclusion, we have observed gate-controlled sign reversal of current noise cross-correlation in two capacitively coupled quantum dots. Our ability to tune the parameters governing transport through the localized states allows us to observe a distinctive noise signature of Coulomb interaction between these states that agrees with the predictions of a simple model.

We thank N. J. Craig for device fabrication and M. Eto, W. Belzig, C. Bruder, E. Sukhorukov, and L. Levitov for valuable discussions. We acknowledge support from the NSF through the Harvard NSEC, PHYS 01-17795,

DMR-05-41988, DMR-0501796, as well as support from NSA/DTO and Harvard University.

- [1] Ya. M. Blanter and M. Büttiker, Phys. Rep. **336**, 1 (2000). Ya. M. Blanter, cond-mat/0511478 (2005).
- [2] T. Martin *et al.*, in *Quantum Noise in Mesoscopic Physics*, NATO Science Series II **97**, edited by Yu. V. Nazarov (Kluwer, Dordrecht, 2003), cond-mat/0209517.
- [3] P. Samuelsson *et al.*, Phys. Rev. Lett. **92**, 26805 (2004).
- [4] C. W. J. Beenakker *et al.*, in *Fundamental Problems in Mesoscopic Physics*, NATO Science Series II **154**, edited by I. V. Lerner, B. L. Altshuler and Y. Gefen (Kluwer, Dordrecht, 2004), cond-mat/0310199.
- [5] A. V. Lebedev *et al.*, Phys. Rev. B **71**, 45306 (2005).
- [6] M. Büttiker, Phys. Rev. Lett. **65**, 2901 (1990); M. Büttiker, Phys. Rev. B **46**, 12485 (1992).
- [7] M. Henny *et al.*, Science **284**, 296 (1999).
- [8] W. D. Oliver *et al.*, Science **284**, 299 (1999).
- [9] S. Oberholzer *et al.*, Physica E **6**, 314 (2000).
- [10] C. Texier and M. Büttiker, Phys. Rev. B **62**, 7454 (2000).
- [11] M. Büttiker, in *Quantum Noise in Mesoscopic Physics*, NATO Science Series II **97**, edited by Yu. V. Nazarov (Kluwer, Dordrecht, 2003), cond-mat/0209517.
- [12] S.-T. Wu and S. Yip, Phys. Rev. B **72**, 153101 (2005).
- [13] S. Oberholzer *et al.*, Phys. Rev. Lett. **96**, 46804 (2006).
- [14] V. Rychkov and M. Büttiker, Phys. Rev. Lett. **96**, 166806 (2006).
- [15] M. P. Anantram and S. Datta, Phys. Rev. B **53**, 16390 (1996).
- [16] T. Martin, Phys. Lett. A **220**, 137 (1996).
- [17] J. Torrès and T. Martin, Eur. Phys. J. B **12**, 319 (1999).
- [18] Y. Chen and R. A. Webb, Phys. Rev. B **73**, 35424 (2005).
- [19] S. S. Safonov *et al.*, Phys. Rev. Lett. **91**, 136801 (2003).
- [20] L. DiCarlo *et al.*, cond-mat/0604018.
- [21] W. G. van der Wiel *et al.*, Rev. Mod. Phys. **75**, 1 (2003).
- [22] I. H. Chan *et al.*, Appl. Phys. Lett. **80**, 1818 (2002).
- [23] L. P. Kouwenhoven *et al.*, in *Mesoscopic Electron Transport*, edited by L. L. Sohn, L. P. Kouwenhoven, and G. Schön (Kluwer, Dordrecht, 1997).
- [24] S. Hershfield *et al.*, Phys. Rev. B **47**, 1967 (1993).
- [25] M. Eto *et al.*, Jpn. J. Appl. Phys. **36**, 4004 (1997).
- [26] G. Kiesslich *et al.*, Phys. Rev. B **68**, 125320 (2003).
- [27] Following the approach of Refs. [24, 25, 26], we define the current matrices as follows: $J_{mn,m'n'}^{tr} = |e|\delta_{nn'}(m - m')W_{mn \leftarrow m'n'}^r$ and $J_{mn,m'n'}^{br} = |e|\delta_{mm'}(n - n')W_{mn \leftarrow m'n'}^r$. The average currents are given by $\langle I_{t(b)} \rangle = \sum_i \langle J_i^{t(b)r} \bar{\rho} \rangle_i$, and the low-frequency correlator by $\langle I_t(\tau) I_b(0) \rangle = \sum_i (\theta(\tau) J_i^{tr} e^{\mathcal{M}\tau} J_i^{br} \bar{\rho} + \theta(-\tau) J_i^{br} e^{\mathcal{M}\tau} J_i^{tr} \bar{\rho})_i$, where θ is the Heaviside step function.
- [28] C. W. J. Beenakker, Phys. Rev. B **44**, 1646 (1991).
- [29] W. Belzig, Phys. Rev. B **71**, R161301 (2005).
- [30] A. Cottet, Phys. Rev. Lett. **92**, 206801 (2004). A. Cottet *et al.*, Phys. Rev. B **70**, 115315 (2004).
- [31] E. V. Sukhorukov *et al.*, Phys. Rev. B **63**, 125315 (2001).
- [32] E. Onac *et al.*, Phys. Rev. Lett. **96**, 26803 (2006).